NUMERICAL SIMULATION AND EXPERIMENTAL INVESTIGATION OF THE PULSE FORMATION IN PASSIVELY Q–SWITCHED Nd:YAG LASERS

Janez Žabkar[1,2], **Marko Marinček**[1,2], **Marko Zgonik**[3,2]

[1]Fotona d.d.
1210 Ljubljana, Stegne 7, Slovenia
[2]'Jožef Stefan' Institute
1000 Ljubljana, Jamova 39, Slovenia
[3]University of Ljubljana, Faculty of Mathematics and Physics
1000 Ljubljana, Jadranska 19, Slovenia

janez.zabkar@fotona.si (Janez Žabkar)

Abstract

We present a theoretical and experimental study of the development of the EM field in pulsed, passively Q–switched solid–state lasers. The rate equations are solved with the Runge–Kutta method separately for the gain medium and a passive Q–switch. In this way, we take the beam propagation and profile variations between the two elements into consideration. With our model, we are able to follow the pulse formation from a randomly generated seed EM field. In the rate equations used, we include excited–state absorption in saturable absorber as well as the pumping term. The latter proves to be important when analyzing the beam profiles when passive Q–switching is used. The formation of the laser afterpulse is observed in the case of stronger pumping. Its intensity profile shows mode structure characteristic of higher order Laguerre–Gaussian beams. Theoretical results are compared with experiment for three different types of laser resonators. In order to obtain a top–hat beam profile, positive–branch unstable resonators with an ordinary and a super-Gaussian output mirror were investigated. Their operation was compared to a plano–concave stable resonator. The calculated beam profiles and temporal developments are in good agreement with the experimental results.

Keywords: computer model, laser beam profile, passive Q–switch, unstable resonators.

Presenting Author's Biography

Janez Žabkar. Janez Žabkar graduated from University of Ljubljana, Faculty of Mathematics and Physics in 2001. Presently he is working in a R&D department at Fotona company, Ljubljana, Slovenia. His main fields of work include nonlinear optics, passively Q–switched lasers and computer modeling. He is working his way towards a PhD in nonlinear optics at University of Ljubljana, Faculty of Mathematics and Physics.

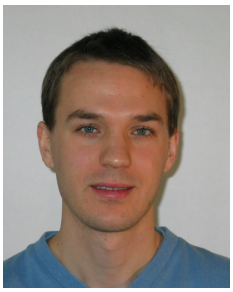

1 Introduction

A laser rod with a large diameter and an optical cavity with a large Fresnel number are required to produce high energy pulses from a Q–switched laser. Such cavities favor, however, laser oscillations in high transverse modes. The result can be a multi–mode laser beam of poor spatial quality. The laser beam quality can be improved using several methods. The use of a positive–branch confocal unstable resonator together with variable-reflectivity mirrors is a widely accepted method [1, 2]. An output coupler with a super–Gaussian reflectivity profile is often used to obtain beams with almost top-hat near–field intensity distribution and low divergence [3]. The combination of a uniform intensity distribution and low divergence is desired in many applications, e.g. for pumping an optical parametric oscillator or in various medical applications. In this paper we present an accurate computer model of a passively Q–switched laser which can correctly predict the output beam intensity profile.

Passively Q–switched lasers employing Cr^{4+}:YAG as a saturable absorber offer the advantage of a very simple design, which leads to small, robust and low-cost systems as compared to actively Q-switched lasers. On the other hand, it is known that in addition to the ground–state absorption, Cr^{4+}:YAG exhibits also absorption in the excited state at the wavelength to be Q–switched [4]. Excited-state absorption is accompanied by short relaxation times from the upper level and hence does not show saturation. Thus, its presence only results in additional loss in the resonator.

The behaviour of passively Q–switched Nd^{3+} lasers with Cr^{4+}:YAG as saturable absorber has been analyzed by a number of authors [5, 6, 7, 8]. However, they mostly deal with optimizing the laser parameters to maximize the output energy and do not investigate the spatial and temporal evolution of laser pulses. Concentrating on analyzing the laser output pulse characteristics (pulse energy, pulse width, peak power), they also neglect the pumping power effect on the output pulse. On the other hand, Anstett et al. [3] take into account the pumping of the laser rod, but don't include a passive Q-switch in their analysis.

Various numerical methods have been proposed to describe the development of EM field in unstable resonators, where diffraction effects play an important role. Among the most efficient methods in terms of computational time is the fast–Fourier transform (FFT) approach, initially proposed by Sziklas and Siegman [9]. Its advantages become most evident when analyzing resonators with multi–mode output profiles.

The model we present in this paper is a modification of that implemented by Marincek et al. [10]. It is based on the calculation of the scalar EM field propagation with the FFT method. Marincek et al. followed the instantaneous beam pattern throughout the laser pulse duration. Some important characteristics of the formation of resonator modes were given in their paper and the influence of the mode competition on the formation of typical beam patterns were analyzed.

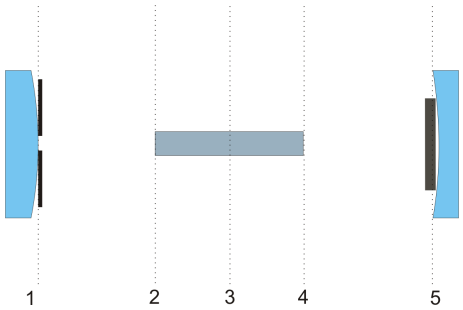

Fig. 1 The model of the laser resonator. The EM field is calculated in each of the computational planes. Planes 1 and 5 represent the output coupler and rear mirror, respectively. A limiting aperture is placed in plane 1,while a passive Q–switch is superimposed in plane 5. Planes 2 and 4 represent laser rod apertures. In plane 3, gain and lensing properties of the laser medium are taken into account.

In the present paper, the two–dimensional FFT has been utilized to study complex profile structures in passively Q-switched lasers of various resonator designs. Since the pulse formation and the beam intensity profile in passively Q-switched lasers are critically influenced by the pumping process, we include a pumping term in the rate equations instead of starting from a high inversion density. In Section II we first present the computational model. The rate equations include the pumping term and excited-state absorbtion in saturable absorber. They are explained in Section III. The results of our simulations are presented in Section IV. The laboratory setup and the experimental results are described in Section V.

2 Computational model

Our goal was that the simulation model would remain simple enough, so the computational time on a regular PC would be acceptable, while taking diffraction properties of light into account to the greatest possible extent.

The resonator scheme in our model is based on the experimental setup. The resonator is divided into 5 computational planes, as shown in Fig. 1. In each plane, there is a grid of 2^8 x 2^8 computational points. The EM field amplitude and phase are monitored at each of these points. The chosen number of lattice points provides sufficient resolution. Further increase in the number of lattice points doesn't influence the final result. The propagation between the neighbouring computational planes is carried out by first calculating a 2–D FFT on the initial field, multiplying the angular spectrum with the appropriate phase factors and then performing the inverse 2–D FFT to obtain the field matrix at the next computational plane.

The computational plane 1 is located at the output mirror. The curvature of the output mirror is represented by a corresponding phase factor. The output mirror reflec-

ISBN 978-3-901608-32-2

tivity *R* and other resonator losses *L*, such as absorption or scattering, are taken into account by multiplying the field amplitude by $\sqrt{R \cdot (1-L)}$. In the case of the variable–reflectivity mirror with a super-Gaussian profile, the reflected field is multiplied by the corresponding factor. A beam–defining pinhole is added in this plane.

The laser rod is described by the next three computational planes 2 – 4. The rod's finite transverse dimensions are represented by the apertures that are placed on the planes at both ends 2 and 4. The edges of all the apertures are smoothed to prevent artificial diffraction caused by the finite lattice division of the computational planes. The gain and lensing properties of the active medium are taken into account in plane 3. The amplitudes of the EM field at each lattice point are calculated from the rate equations. A thin lens in this plane is used to simulate thermal lensing of the rod by multiplying the EM field with an appropriate phase factor. Changing the focal length of the lens simulates different thermal load conditions.

Plane 5 contains the passive Q–switch and the rear mirror. During the formation of the pulse, the transmission of the Q–switch is calculated based on the intensity of the local EM field. Following is the reflection off the rear mirror, where the mirror radius is taken into account by multiplying the field by a corresponding phase factor.

The calculation begins in plane 3. The EM field starts to build up from spontaneous emission whose contributions are superimposed, with random phase, at each lattice point. The amplitudes of spontaneous emission contributions are determined by population inversion, spontaneous emission lifetime and geometrical properties of the laser rod and resonator. Because of the random initialization of the EM field, the numerical model doesn't favor any particular initial profile symmetry. We follow the development of the generated field towards both mirrors. This means that two counter–propagating field planes E_{L} and E_{R} are propagated through the resonator simultaneously, instead of only one. By using two field planes, we achieve higher temporal resolution, since the field planes reach the output coupler twice per full resonator round–trip time. The rate equations that govern the amplification of the laser beam are explained in greater detail in the next section.

3 Rate Equations

In the present paper we follow the rate equations of Zhang et al. [6] who modeled passively Q–switched lasers and included excited state absorption of the saturable absorber in their analysis. In order to simulate also the temporal development of the laser pulse, we modified their equations to include also the pumping term. Additionally, we solve the rate equations separately for the gain medium and a passive Q–switch, thus accounting for the beam profile variations between the two planes.

In every computational step, first the spontaneous emission contribution to EM field is calculated with the following difference equation:

$$\Delta|E_{\mathrm{sp}}|^2 = \frac{2h\nu t_0}{n_{\mathrm{rod}}\epsilon_0}\frac{N}{\tau_{\mathrm{rod}}}\,\Delta\tau \qquad (1)$$

where *h* is the Planck's constant, ν is the frequency of light, t_0 is the time interval equal to one half of the resonator round trip time, *N* is the gain medium inversion density, n_{rod} is the gain medium refractive index, ϵ_0 is the permittivity of free space, τ_{rod} is the upper laser level lifetime, and $\Delta\tau = 1$ where we have introduced the normalized time $\tau = \frac{t}{t_0}$.

The rate equations describing the interaction of the EM field with the laser rod are as follows:

$$\frac{\mathrm{d}N}{\mathrm{d}\tau} = -\frac{\sigma c_0 \epsilon_0 n_{\mathrm{rod}}}{2h\nu}\, t_0 \cdot N\,|E|^2 + \\ + W_{\mathrm{p}}\, t_0\,(N_{\mathrm{tot}} - N) \qquad (2)$$

$$\frac{\mathrm{d}|E|^2}{\mathrm{d}\tau} = \sigma c_0 \frac{d_{\mathrm{rod}}}{d_{\mathrm{res}}}\, t_0 \cdot N\,|E|^2 = \alpha^2|E|^2 \qquad (3)$$

where $|E|^2 = |E_{\mathrm{L}}|^2 + |E_{\mathrm{R}}|^2$ is the incoherent addition of the two counter-propagating fields, σ is the gain medium stimulated emission cross section, c_0 is the speed of light in vacuum, W_{p} is the pumping rate, N_{tot} is the Nd ion density, d_{rod} is the laser rod length, and d_{res} is the cavity optical length. The gain medium rate equations are solved with a fourth–order Runge–Kutta method every time both field planes meet in the central computational plane. Since one computational step accounts for $t_0 = 0.44\,\mathrm{ns}$ and the FWHM of the temporal pulse profile is about 7 ns, we refine the step in the Runge–Kutta method to one tenth of t_0 to improve precision.

The first term in (2) represents the inversion population depletion by stimulated emission and the second term accounts for the pumping of the active medium. The reduction of the inversion density due to spontaneous emission is neglected. Equation (3) represents the amplification by stimulated emission. In the second part of (3) the single pass amplitude amplification factor α is defined.

The result of the amplification in the central computational plane is then given as

$$E_{\mathrm{L,R}}(t + t_0) = \alpha E_{\mathrm{L,R}}(t) + \Delta|E_{\mathrm{sp}}|e^{i\phi} \qquad (4)$$

for both counter-propagating field planes E_{L} and E_{R}. In (4), ϕ is a random phase between 0 and 2π. The stimulated and spontaneous emission terms are written separately to emphasize that the spontaneous emission is superimposed with a random phase, while the stimulated emission is added in–phase.

The Cr^{4+} energy levels in the Cr:YAG Q–switch are shown in Fig. 2. Starting from the ground level (L1) absorption of a photon excites the Cr^{4+} to a higher energy level L3. The relaxation from L3 to level L2 is fast. The lifetime of L2 is long compared to the pulse duration and was taken to be $\tau_{\mathrm{sa}} = 4\,\mu s$ [6]. The excited state absorption shifts Cr^{4+} from L2 to L4. The

ISBN 978-3-901608-32-2

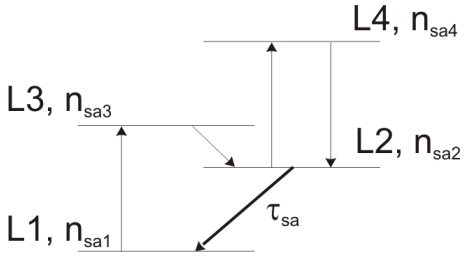

Fig. 2 Energy-level diagram for a saturable absorber indicating both the ground– and excited–state absorption transitions. n_{sai} indicates population density of level *i* (Li). Transitions from levels L3 and L4 to L2 are fast, so the entire absorbing population is divided between levels L1 and L2. The lifetime of L2 (τ_{sa}) is long compared to the pulse duration and was taken to be $\tau_{\mathrm{sa}} = 4\,\mu s$.

ions decay from L4 back to L2 via radiationless processes. Since the decay from L3 and L4 is fast, the absorbing population is effectively divided only between L1 and L2, giving $n_{\mathrm{sa0}} = n_{\mathrm{sa1}} + n_{\mathrm{sa2}}$, where n_{sa0} is the density of Cr^{4+}, while n_{sa1} and n_{sa2} are the ground and excited state population densities, respectively. The equations that govern the EM field and the saturable absorber ground state population density are the following:

$$\frac{\mathrm{d}|E|^2}{\mathrm{d}\tau} = -\sigma_{13} c_0 \frac{d_{\mathrm{sa}}}{d_{\mathrm{res}}}\, t_0 \cdot |E|^2\, n_{\mathrm{sa1}} - \sigma_{24} c_0 \frac{d_{\mathrm{sa}}}{d_{\mathrm{res}}}\, t_0 \cdot |E|^2\, (n_{\mathrm{sa0}} - n_{\mathrm{sa1}}) \quad (5)$$

$$\frac{\mathrm{d}n_{\mathrm{sa1}}}{\mathrm{d}\tau} = -\frac{\sigma_{13} c_0 n_{\mathrm{sa}} \epsilon_0}{2h\nu}\, t_0 \cdot |E|^2\, n_{\mathrm{sa1}} + t_0\, \frac{n_{\mathrm{sa0}} - n_{\mathrm{sa1}}}{\tau_{\mathrm{sa}}} \quad (6)$$

where σ_{13} and σ_{24} are the ground and excited state absorption cross sections, respectively, d_{sa} is the thickness, n_{sa} is the refractive index and τ_{sa} is the excited state lifetime.

The terms in (5) represent the EM field absorption in the saturable absorber ground and excited-state, respectively. The terms in (6) represent the depletion of the ground level population by absorption and repopulation by relaxation from L2. These rate equations are solved every time a field plane reaches plane 5.

4 Computational results

The values of the laser parameters used in our model are as follows: the laser rod is a 1% doped Nd:YAG crystal. It is 5 cm long with a diameter of 3 mm. The Nd ion density $N_{\mathrm{tot}} = 1.38 \cdot 10^{26}\mathrm{m}^{-3}$. The stimulated emission cross section $\sigma = 2.8 \cdot 10^{-23}\mathrm{m}^2$ and the upper laser level lifetime $\tau_{\mathrm{rod}} = 230\mu\mathrm{s}$ [11]. The resonator is 9 cm long resulting in one half of the resonator round trip time (t_0) being $0.44\,\mathrm{ns}$. The diameter of a limiting aperture is 2.2 mm and the pumping rate $W_{\mathrm{p}} = 50\ s^{-1}$. The absorption cross sections $\sigma_{13} = 4.3 \cdot 10^{-18}\mathrm{cm}^2$ and $\sigma_{24} = 8.2 \cdot 10^{-19}\mathrm{cm}^2$ [6]. The refractive indices of the gain medium and the Q–switch are 1.82. The thickness of the Q–switch $d_{\mathrm{sa}} = 0.13$ cm. Its optical density was chosen to be 0.3 or equivalently, its initial transmission $T_0 = 0.52$. Using these parameters, the density of Cr ions $n_{\mathrm{sa0}} = -\frac{ln\ T_0}{\sigma_{13} d_{\mathrm{sa}}} = 1.16 \cdot 10^{18}\mathrm{cm}^{-3}$.

Three different types of resonators were investigated. The resonator A was a plano–concave stable resonator with the rear mirror radius of -10 m. The resonator B was an unstable resonator with mirror radii of -20 m and 5 m for the rear mirror and output coupler, respectively. The resonator C was also an unstable resonator with mirrors having the same curvatures as those in case B, but the output coupler had a super–Gaussian reflectivity profile of the form $R_0\, exp[-\left(\frac{r}{w}\right)^6]$ with the central reflectivity $R_0 = 0.4$ and $w = 1$ mm.

During the simulation, the instantaneous near–field intensity profile was monitored continuously. To obtain the overall energy density profile, the instantaneous beam intensity distributions were integrated during the simulation.

The spatio–temporal evolutions of the laser pulses in the three resonators are shown in Fig. 3. In all three resonators the pulse starts to develop on the axis. In case A, the profile in the first part of the pulse generation is centrally peaked. In the second part of the evolution, there are also some higher–order modes present. In the resonator B, after the pulse develops the central, Gaussian–like peak, it broadens rapidly and forms ring–shaped profiles in the second part of the temporal evolution. A similar course of events is seen in the resonator C, but the development is much smoother. The gradual broadening of the ring–shaped profiles results in an almost top–hat energy density profile of the laser pulse.

Fig. 4 shows the calculated beam energy density profiles for all three types of resonators investigated. In resonator A, the laser pulse shows a strong central maximum. The unstable design of resonator B produces a circular pattern that shows a zero in radial intensity profile, roughly like a TEM_{10} mode in cylindrical coordinates. In the third case, the laser profile becomes similar to a top–hat profile. Such a flat intensity profile is preferred in many applications. We should stress, however, that while the integrated intensity profile is top–hat, the instantaneous intensity profiles are not. This is an important result, especially for nonlinear optics.

The model was put to an additional test by calculating the second laser pulse, which may form in the case of prolonged pumping beyond the formation of the first pulse. The time evolution of the second pulse in resonator A is shown in Fig. 6. Its profile turned out to be of a very high order ($TEM_{0\,20}$). This kind of pattern was only observed in the case of a stable resonator A. The calculated energy density profiles of the first and second laser pulse are shown in Fig. 5. The initial uniform inversion density is strongly depleted on the axis of the laser rod when the first pulse is generated. Because of the short excited state relaxation time, the Q–switch closes and further pumping is raising the inver-

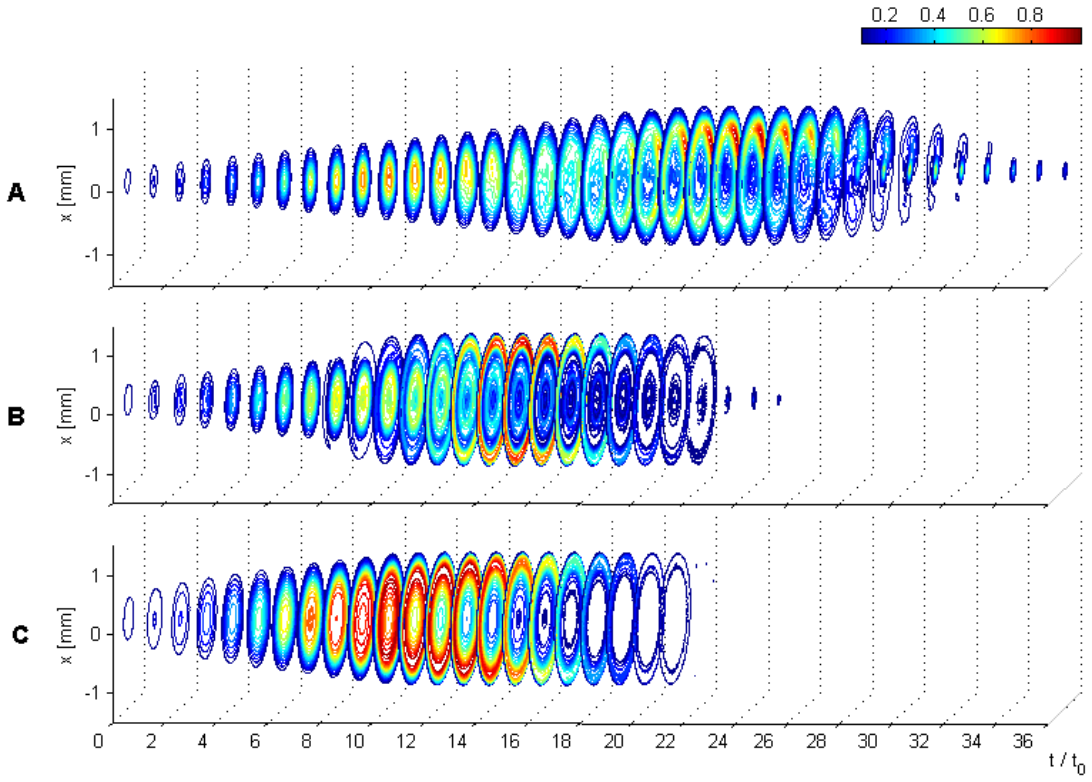

Fig. 3 The temporal evolution of the laser pulses in three types of resonators: A) stable resonator, B) unstable resonator, C) unstable resonator with a super–Gaussian reflectivity output coupler. In the case of a stable resonator, the pulse is initially almost Gaussian, with higher–order modes present in the later part of the pulse formation. In the other two cases, the ring–shaped profiles are formed which spread from the center to the edge of the laser rod. When utilizing a super–Gaussian output coupler, this broadening is smooth, which results in an almost flat, top–hat intensity profile.

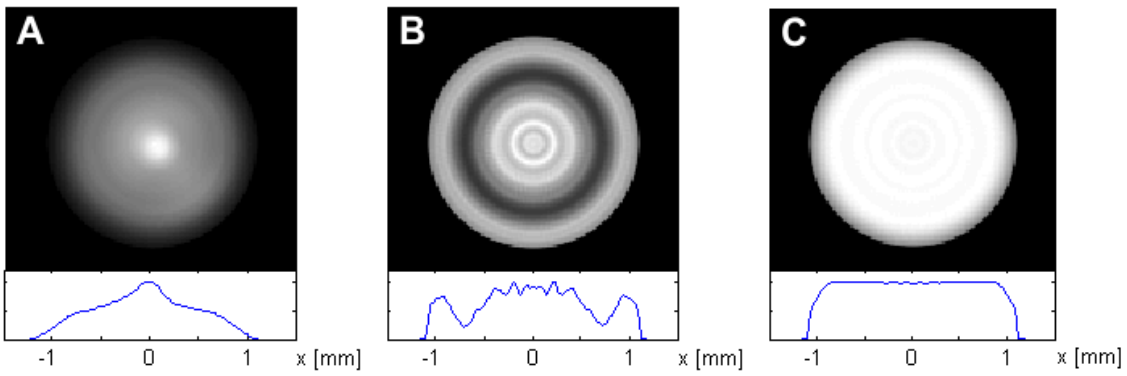

Fig. 4 The calculated near–field energy density profiles for three different types of resonators: A) stable resonator, B) unstable resonator, C) unstable resonator with a super–Gaussian reflectivity profile. Below are the cross-sections through the centers of the profiles. The profiles are changed from a centrally peaked profile A to a TEM_{10}–like profile B and to a top–hat profile C. The figures are normalized.

ISBN 978-3-901608-32-2

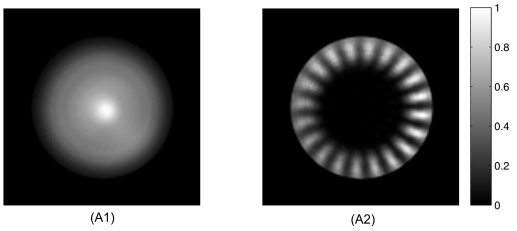

Fig. 5 The calculated energy density profiles of the first (A1) and the second (A2) laser pulse in the case of the stable laser resonator A. Since the first pulse depletes the inversion population in the central section of the laser rod, the second pulse is generated by the outer section of the rod, resulting in a very high–order mode.

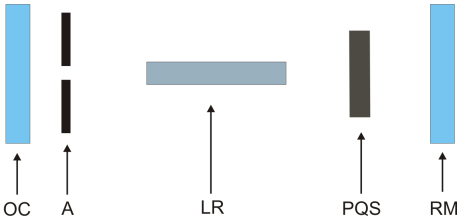

Fig. 7 The laboratory laser configuration. LR - Nd:YAG laser rod, PQS - Cr:YAG passive Q-switch, A - aperture, OC - output coupler, RM - rear mirror.

sion population uniformly throughout the laser rod. After about 10 μs of pumping, the inversion density in the outer part of the rod has reached high enough level and the second laser pulse is generated. This mechanism produces the circular shape of the second laser pulse. In the resonators B and C the second pulse doesn't exhibit such a profile. Obviously, the first pulse depletes the inversion density more homogenously.

5 Experimental setup

To verify our computational model, the subject of experimental investigations was a compact, passively Q-switched, flashlamp pumped Nd:YAG laser schematically shown in Fig. 7. The laser consists of the same components as our model laser and has the same parameters apart from the position of the aperture and the Q–switch. The same three resonator configurations A, B and C were tested and compared. For each of the resonator types, we measured the spatial profile of the laser beam in the near-field as well as in the far–field of the laser. The shape and size of the beams were measured with a digital camera. The beam diameters were calculated from the recorded beam profiles using the second-moment method as described in [12].

The measured beam profile in resonator A is shown in Fig. 8A. The beam profile exhibits a central peak, however it is more pointed than a Gaussian profile. The beam profile in resonator B is shown in Fig. 8B. The profile is distinctly different from the stable resonator case. It has a strong central maximum, a circular minimum and another peak at the outer edge of the profile.

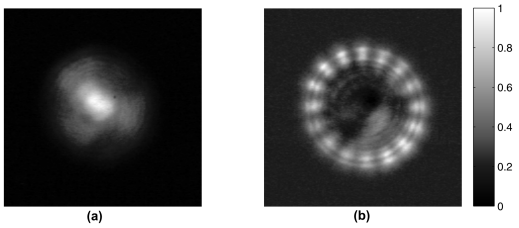

Fig. 9 The measured intensity profiles of the first and the second laser pulse. The profile of the second laser pulse was obtained by subtracting the measured profile of the first pulse from the measured profile of a double pulse. Very good agreement with the calculated profiles of Fig. 5 can be observed.

For the resonator C we used identical mirror radii as in the case B, with a super-Gaussian reflectivity profile on the output coupler, as described in Section IV. The laser beam profile has changed to almost top-hat, with only a slight maximum at the outer edge of the beam, as shown in Fig. 8C. Compared to the results of our computer model in Fig. 4, a very good agreement is achieved between calculated and experimental profiles.

In order to produce two consecutive pulses, the pumping was increased. We measured the near–field beam profile of a double pulse with a camera and then subtracted the profile of a single pulse to obtain the second pulse shape. To minimize the difference in thermal lensing between the two measurements, we only fired a few shots in this double–pulse regime and then return to the single–pulse operation. The measured laser beam profiles of the first and second laser pulse are shown in Fig. 9. A very good agreement with the predicted profiles from Fig. 5 can be observed.

We wanted to confirm experimentally also the predicted time evolution of the pulse in the case of the resonator C, where the beam evolves from the center. We measured the temporal dependence of the total laser pulse and that of a laser pulse transmitted through an aperture centered on the axis. Its diameter was 0.5 mm, so only the central part of the beam was transmitted. Both temporal dependences are shown in Fig. 10. The difference clearly shows that the outer part of the pulse evolves later which agrees with our calculation.

6 Conclusion

A computational model was developed in order to study the development of the EM field in passively Q–switched Nd:YAG lasers. The model enables us to follow the formation of a laser pulse as it is generated from a randomly generated spontaneous initial field.

Our model gives similar results when run several times with the same parameters. Three different types of laser resonators were investigated with our model. The results were verified with experimental measurements made on equivalent laser resonators. Very good agreement between the calculated and experimental intensity

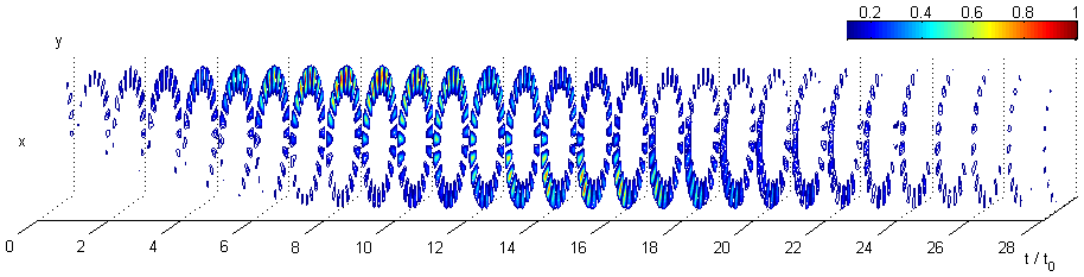

Fig. 6 The temporal development of the second laser pulse in a stable laser resonator. The formation of a high–order mode can be clearly seen.

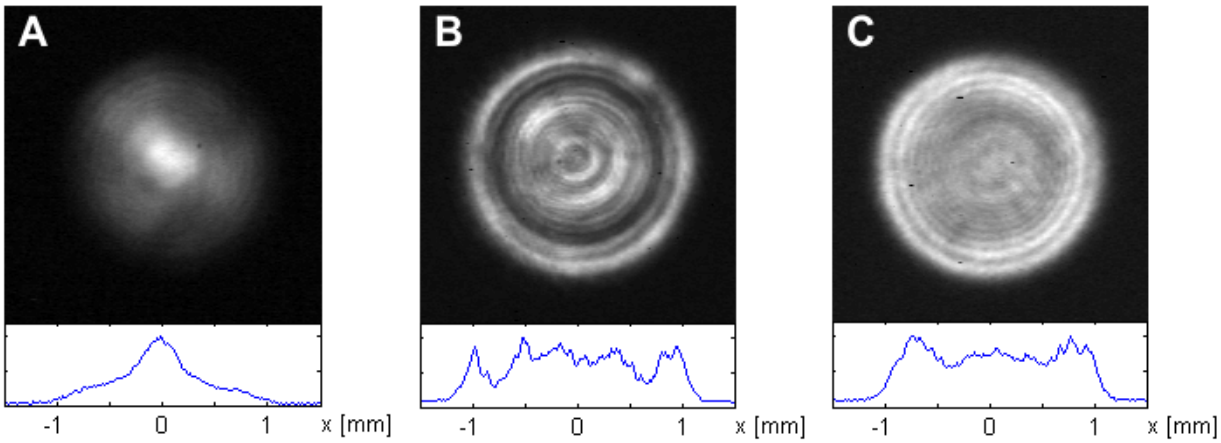

Fig. 8 A) Measured beam profile for a plano-concave stable resonator with rear mirror radius of -10 m. B) Measured beam profile for an unstable resonator with mirror radii of -20 m and 5 m for a rear mirror and output coupler, respectively. The beam profile resembles TEM_{10} mode with a central maximum, a circular minimum and a circular peak at the outer edge of a beam. C) Measured beam profile for an identical unstable resonator to case B, but with a super-Gaussian reflectivity output coupler. The beam profile is now almost top-hat, with only a slight peak at the outer edge of the beam. Below the profiles are the cross-sections through the centers of the profiles.

ISBN 978-3-901608-32-2

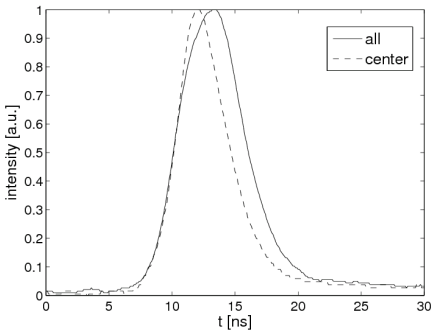

Fig. 10 Temporal development of the total laser power and the power measured through a 0.5 mm diameter pinhole. The time duration of a central section of a beam is shorter than the duration of a whole pulse, indicating that during the pulse formation the central section of the profile decays sooner than the rest. This confirms the calculated temporal evolution of a pulse in such a resonator.

profiles was observed. The temporal evolution of a laser pulse was investigated, as well. The formation of the second laser pulse was an additional test of our model. The calculated intensity profile of the second pulse is in very good agreement with the measured profile. The results of our model were confirmed with experimental measurements.

7 References

[1] A. Caprara, G. C. Reali. Time-resolved M^2 of nanosecond pulses from a Q-switched variable-reflectivity-mirror Nd:YAG laser. *Opt. Lett.*, 17(6): 414-416, 1992.

[2] S. De Silvestri, V. Magni, S. Taccheo, G. Valentini. Q-switched Nd:YAG laser with super-Gaussian resonators. *Opt. Lett.*, 16(9): 642-644, 1991.

[3] G. Anstett, M. Nittmann, A. Borsutzky, R. Wallenstein. Experimental investigation and numerical simulation of the spatio-temporal dynamics of nanosecond pulses in Q-switched Nd:YAG lasers. *Appl. Phys. B*, 76: 833-838, 2003.

[4] M. Hercher. An Analysis of Saturable Absorbers. *Appl. Opt.*, 6(5), 1967

[5] J. J. Degnan. Optimization of Passively Q-Switched Lasers. *IEEE J. Quantum Electron.*, 31: 1890-1901, 1995.

[6] X. Zhang, S. Zhao, Q. Wang, Q. Zhang, L. Sun and S. Zhang. Optimization of Cr^{4+}-Doped Saturable-Absorber Q-Switched Lasers. *IEEE J. Quantum Electron.*, 33: 2286-2294, 1997.

[7] G. Xiao and M. Bass. A Generalized Model for Passively Q-switched Lasers Including Excited State Absorbtion in the Saturable Absorber. *IEEE J. Quantum Electron.*, 33: 41-44, 1997.

[8] F. D. Patel and R. J. Beach. New Formalism for the Analysis of Passively Q-Switched Laser Systems. *IEEE J. Quantum Electron.*, 37: 707-715, 2001.

[9] E. A. Sziklas, A. E. Siegman. Mode calculations in unstable resonators with flowing saturable gain. 2: Fast Fourier transform method. *Appl. Opt.*, 14(8): 1874-1889, 1975.

[10] M. Marincek, M. Copic, M. Lukac. Time-Dependent EM Field Characterization in Pulsed Lasers. *IEEE J. Quantum Electron.*, 36: 502-508, 2000.

[11] W. Koechner, *Solid-State Laser Engineering*, 5th ed., Springer-Verlag, Berlin, Germany, 1999.

[12] ISO 11 146-1. Lasers and laser-related equipment - Test methods for laser beam widths, divergence angles and beam propagation ratios - Part 1: Stigmatic and simple astigmatic beams. Geneva, 2005.

